Collagen and myosin characterization by orientation field second harmonic microscopy

Christophe Odin[1], Thomas Guilbert[1], Alia Alkilani[1], Olena P. Boryskina[1,2], Vincent Fleury[1], and Yann Le Grand[1]

[1] *Institut of Physics of Rennes IPR/UMR CNRS 6251, University of Rennes I, Campus de Beaulieu, Bat 11A, 35042 Rennes Cedex, FRANCE*
[2]*Institute of Radiophysics and Electronics NAS of Ukraine, 12Acad. Proskura str., Kharkov, 61085, Ukraine*

christophe.odin@univ-rennes1.fr

Abstract: Collagen and myosin fibrils are endogenous harmonophores that both give rise to Second Harmonic Generation (SHG). By combining four polarization SHG images provided by a scanning microscope, we show that the orientation of the principal axis of the nonlinear susceptibility tensor $\chi^{(2)}$ can be determined for each pixel of the image. The ratio $\rho = \chi_{33}/\chi_{15}$ of the principal components of $\chi^{(2)}$ of collagen and myosin was obtained with the same method, and found within the range $1.6 - 1.8$ and $0.5 - 0.6$ respectively. The orientation of the principal axis of $\chi^{(2)}$ is shown to be correlated to the orientation of the fibrils themselves. This provides a straightforward method, which we call Orientation Field-Second Harmonic Microscopy (OF-SHM), to reconstruct orientation fields of fibrils at various scales and resolutions in different biological systems (from muscle sarcomere to the whole embryo).

References and links

1. K. Kroy, "Elasticity, dynamics and relaxation in biopolymer networks," Curr. Op. Coll. & Int. Sc. **11**, 56-84 (2006).
2. G.A. Holzapfel "Computational Biomechanics of Soft Biological Tissue," in Encycl. Comput. Mech. E. Stein, R. de Borst and T.J.R. Hughes eds (John Wiley & Sons, Ltd, Chichester, 2004) **2**, 605-635.
3. K. König, "Multiphoton microscopy in life sciences," J. Microsc. **200**, 83-104 (2000).
4. W.R. Zipfel, R. M. Williams, and W.W. Webb, "Nonlinear magic : multiphoton microscopy in the biosciences," Nat.Biotechnol. **21**, 1369-1377 (2003).
5. P. J. Campagnola and L. M. Loew, "Second-harmonic imaging microscopy for visualizing biomolecular arrays in cells, tissues and organisms," Nat. Biotechnol. **21**, 1356-1360 (2003).
6. D. Débarre, A.-M. Pena, W. Supatto, T. Boulesteix, M. Strupler, M.-P. Sauviat, J.-L. Martin, M.-C. Schanne-Klein and E. Beaurepaire, "Second-and third-harmonic generation microscopies for the structural imaging of intact tissues,M/S : médecine sciences, **22**, 845-850 (2006).
7. V. Le Floc'h, S. Brasselet, J.-F. Roch, and J. Zyss, "Monitoring of Orientation in Molecular Ensembles by Polarization Sensitive Nonlinear Microscopy," J. phys. Chem. B **107**, 12403-12410 (2003).
8. S. Brasselet, V. Le Floch, F. Treussart, J.-F. Roch, J. Zyss, E. Botzung-Appert, and A. Ibanez,"In Situ Diagnostics of the Crystalline Nature of Single Organic Nanocrystals by Nonlinear Microscopy," Phys. Rev. Lett. **92**, 207401-207404 (2004).
9. S. Brasselet, J. Zyss, "Nonlinear polarimetry of molecular crystals down to the nanoscale," C. R. Physique R. Adv. Cryst. Opt. **8**, 165-179 (2007).

10. P. Stoller, K.M. Reiser , P. M. Celliers, and A. M. Rubenchik, "Polarization-Modulated Second Harmonic Generation in Collagen," Biophys. J. **82**, 3330-3342 (2002).
11. S.W. Chu, S. Y. Chen, G. W. Chern, T.H. Tsai, Y.C. Chen, B. L. Lin, and C.K. Sun. "Studies of $\chi(2)/\chi(3)$ tensors in submicron-scaled bio-tissues by polarization harmonics optical microscopy," Biophys. J. **86**, 3914-3922 (2004).
12. W.R. Zipfel, R. M. Williams, R. Christie, A. Y. Nikitin, B. T. Hyman and W.W. Webb. "Live tissue intrinsic emission microscopy using multiphoton-excited native fluorescence and second harmonic generation," Proc. Natl. Acad. Sci. USA. **100**,7075-7080 (2003).
13. A. Zoumi, A. Yeh, and B. J. Tromberg, "Imaging cells and extracellular matrix in vivo by using second-harmonic generation and two-photon excited fluorescence," Proc. Nat. Acad. Sc. **20**, 11014-11019 (2002).
14. T. Boulesteix, E. Beaurepaire, M. Sauviat, and M.-C. Schanne-Klein, " Second-harmonic microscopy of unstained living cardiac myocytes:measurements of sarcomere length with 20-nm accuracy," Opt. Lett. **29**, 2031-2033 (2004). http://www.opticsinfobase.org/abstract.cfm?URI=ol-29-17-2031
15. S.V. Plotnikov, A. C. Millard, P. J. Campagnola, and W. A. Mohler, "Characterization of the myosin-based source for second-harmonic generation from muscle sarcomeres," Biophys J. **90**,693-703 (2006).
16. S.T. Jiang, "Contribution of Muscle Proteinases to Meat Tenderization," Proc. Nat. Sc. Council, ROC, Part B **22**, 97-107 (1998).
17. C. Odin, Y. Le Grand, A. Renault, L. Gailhouste, and G. Baffet, "Orientation fields of nonlinear biological fibrils by second harmonic generation microscopy," J. Microsc. **229**, 32-38 (2008).
18. S. Roth and I. Freund, "Second harmonic generation in collagen," J. Chem. Phys. **70**, 1637-1643(1979).
19. R.M. Williams,W.R. Zipfel, and W. W. Webb, "Interpreting Second-Harmonic Generation Images of Collagen I Fibrils," Biophys. J. **88**, 1377-1386 (2005).
20. P. Fratzl,"Cellulose and collagen: from fibres to tissues," Curr. Op. Coll. Int. Sc. **8**, 32-39 (2003).
21. D. A. Kleinman, "Nonlinear Dielectric Polarization in Optical Media," Phys. Rev. **126**, 1977-1979 (1962).
22. F. Tiaho, G. Recher, and D. Rouède, "Estimation of helical angles of myosin and collagen by second harmonic generation imaging microscopy," Opt. Express **15**, 12286-12295 (2007). http://www.opticsinfobase.org/abstract.cfm?URI=oe-15-19-12286
23. X. Han, R. M. Burke, M. L. Zettel, P. Tang, and E. B. Brown, "Second harmonic properties of tumor collagen: determining the structural relationship between reactive stroma and healthy stroma," Opt. Express **16**, 1846-1859 (2008). http://www.opticsinfobase.org/abstract.cfm?URI=oe-16-3-1846
24. C. Odin, "NMR studies of Phase Transitions," Ann. Rep. NMR Spectr., G. Webb ed (Elsevier/North-Holland, Amsterdam, 2006) **59**, 117-205.
25. L. Gao, L. Jin, P. Xue, J. Xu, Y. Wang, H. Ma, and D. Chen, "Reconstruction of complementary images in second harmonic generation microscopy," Opt. Express **14**, 4727-4735 (2006). http://www.opticsinfobase.org/abstract.cfm?URI=oe-14-11-4727
26. H. Hamburger, and H.L. Hamilton "A series of normal stages in the development of the chick embryo," J.Morphol. **88**, 49-92 (1951).
27. K. V. Mardia and P. E. Jupp, *Directional Statistics*" (John Wiley and Sons Ltd, Chichester, 2000).
28. P. J. Elbischger, H. Bischof, P. Regitnig and G. A. Holzapfel, "Automatic analysis of collagen fiber orientation in the outermost layer of human arteries," Pattern Anal Applic **7**, 269-284 (2004).
29. M.H. Stromer, D.E. Goll, R.B. Young, R.M. Robson and F.C. Parrish, "Ultrastructural features of skeletal muscle differentiation and development," Jr. J. Anim Sci. **38**, 1111-1141 (1974).
30. A. Leray, L. Leroy, Y. Le Grand, C. Odin, A. Renault, V. Vié, D. Rouède, T.Mallegol, O.Mongin,M. H. V.Werts and M. Blanchard-Desce, Organization and orientation of amphiphilic push-pull chromophores deposited in Langmuir-Blodgett monolayers studied by second-harmonic generation and atomic force microscopy, Langmuir **20**, 8165-8171 (2004).
31. O. P. Boryskina, Y. Le Grand, C. Odin and V. Fleury, "The role of distribution and orientation of collagen fibers in tissue development: study by means of double imaging by two-photon excited fluorescence and second harmonic generation microscopy", Proc Europ. Microw. Assoc. **4**, 255-259 (2008).
32. M.L. Concha and R.J. Adams, "Oriented cell divisions and cellular morphogenesis in the zebrafish gastrula and neurula: a time-lapse analysis," Development **125**, 983-994 (1998).

1. Introduction

Most biological tissues possess some degree of order, that determines their flexibility and elasticity [1]. These properties are essential in the evolution of multicellular organisms, because they control transport of fluids, nutrients and oxygen, and endow an ability to respond to changing environment. For instance, soft connective tissues such as skin structure protect organs, while tendons or blood vessels connect organs. A primary role is to transmit force or equilibrate pressures. Thus all these structures need to support strong mechanical stresses and strains,

such as blood vessels dilations due to blood pulse waves. Being complex fiber-reinforced composite structures, their rheological properties depend on structural organization and features, from the microscopic to macroscopic level [2]. Therefore, there is a need to understand both the biological and mechanical characteristics of the cells and extracellular matrix that comprise a tissue or an organ. In particular, the fibrous content leads to highly anisotropic properties, and one of the motivations of this work was to image the orientation and amplitude of the nonlinear susceptibility tensor of fibrillar biomaterials.

Due to the difficulties in accurately visualizing the *in-depth* microstructure of biological tissues, recent attention has been devoted to non-destructive multiphoton microscopy techniques. Nonlinear excitation provides now a large panel of imaging applications [3, 4], based on Two-Photon Excitation Fluorescence (TPEF) and Second Harmonic Generation (SHG) phenomena. The inherent localization of the nonlinear excitation at the objective focal volume provides intrinsic optical sectioning and high in-depth penetration (up to 500 μm) to point-scanning microscopy despite of scattering, while drastically reducing out-of-focus photobleaching and phototoxicity [5, 6]. TPEF/SHG microscopy is therefore well suited for *in situ* and *in vivo* studies. In particular, TPEF is an incoherent process whose contrast is proportional to the concentration of fluorophores, while SHG is a coherent phenomenon that arises from supramolecules deprived of center of inversion (harmonophores) and organized in noncentrosymmetrical mesoscopic structures. Combining TPEF and SHG contrasts, as well as their polarization dependence, give a lot of information about harmonophore organization [7, 8, 9]. As a consequence of the coherent nature of SHG, the contrast is proportional to the square of the concentration of harmonophores, and is strongly dependent on order and polarization [10, 11]. Moreover, cells and Extra Cellular Matrix (ECM) include a variety of biological macromolecules that give rise to *endogenous* TPEF and SHG signals [12], allowing multiphoton imaging without staining. In addition, fibrous proteins such as type-I collagen and myosin are the main sources of SHG in living tissues [5, 13, 15].

Due to the complexity of the nonlinear interactions, interpretation of TPEF and SHG image contrasts on physical grounds is not straightforward. In particular, determination of the orientation fields of fibrils or bundles of fibrils is a ticklish problem. This difficulty, and the complementarity of TPEF and SHG microscopies is illustrated by the high magnification images of veal muscle presented in Fig. 1 with a RGB color coding. As shown in the theoretical section, the average of four images acquired at input laser polarizations 0, 45, 90 and 135 $^\circ$ provides a contrast that is independent of the orientation of the fibrils. The striated appearance of the myofibrils due to a segmentation over basic contractile units (sarcomeres) is readily observable as alternating bands Fig. 1(a-f), both in the TPEF and SHG images [14]. This unique feature is a direct consequence of the precise alignment of the filament systems of the sarcomeres. It was shown that SHG mostly arises from the myosin-containing thick filaments [15], and does not require an overlap with actin filaments.

With the RGB coding used in this presentation, colocalized signal intensities with almost same weights would give a yellow color. But as indicated by the images of Fig. 1(c) and (f), the red and green colors almost not superimposed, the SHG red bands being in between the TPEF green bands. This alternating structure can be quantified by performing line sections. For instance, a line section over the TPEF and SHG images along the fibrils is shown in Fig. 1(g) : the TPEF and SHG signals alternate in antiphase along the fibril axis, with a separation between two maxima within $2.7 - 2.9$ μm. The spatial FFT of line sections of length $\sim 65 \mu$m are shown in Fig. 1(h). A sharp peak at ≈ 0.358 μm^{-1} (that corresponds to a period of 2.8 μm) is observed for both TPEF and SHG signals, indicating the almost perfect periodicity of the array of sarcomeres along myofibrils. This period is an estimate of the sarcomere length for this sample. For meat, the sarcomere length determines meat tenderness [16].
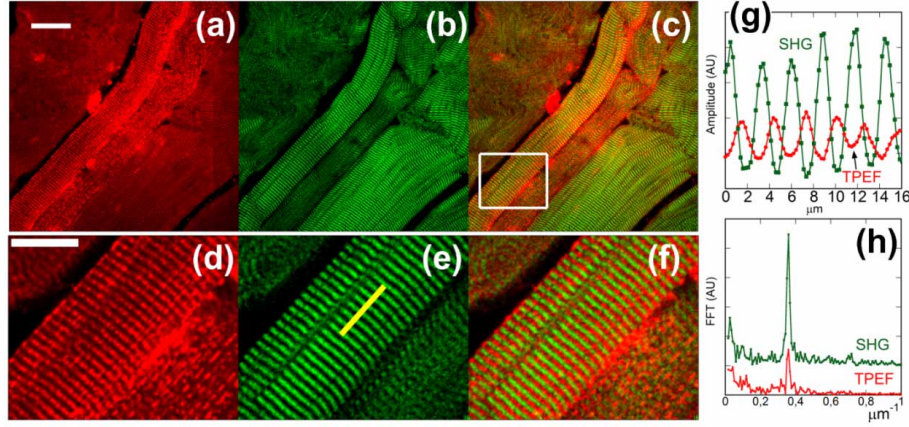
Fig. 1. (color online) : Colocalization of TPEF and SHG signals on veal fresh muscle with a RGB color coding. Full scale 1024x1024 images, 60xW-NA1.2 objective : (a) TPEF (red); (b) Isotropic SHG from Myosin (green); (c) TPEF+SHG (red and green) RGB image. Scale bar : 40μm. (d-e-f) Zoom corresponding to the white rectangle in image (c), scale bar : 20μm. (g) Sections of the TPEF and SHG images along the bundle of myofibrils; (h) Spatial Fourier transforms of 65μm sections.

A close inspection of the image of Fig. 1(e) reveals that the dark bands are not perpendicular to the apparent myosin bundle anywhere. This observation emphasizes the need for a method that measures the fibril orientation independently of the intensity contrast in the image.

We recently proposed the principle of a method [17] to map the orientation of nonlinear fibrils in biological structures, independently of the contrast of the image. Indeed, using a combination of only four SHG images, we demonstrated that the individual collagen fibers from rat liver ECM and the corresponding orientation of the principal axis of the nonlinear susceptibility tensor are parallel. In this article, we develop further our SHG polarimetric method. The goal of this work was to assess the feasibility and reliability of quantifying the orientation of collagen and myosin fibrils in different tissues where fibrils form *dense* arrays, at various optical resolutions. We also indicate how the ratio of the components of the nonlinear susceptibility tensor $\chi^{(2)}$ ($\rho = \chi_{zzz}/\chi_{zxx}$ for axial systems) can be derived from this method by means of histograms. Application to various biological samples containing collagen or myosin emphasizes the versatility of the method.

2. Theory of SHG polarization analysis and image analysis

The physical grounds of polarization analysis of collagen structures using SHG response can be found for instance in [10, 18, 19]. The main formula and the principles of our method [17] are summed up in this part.

Second harmonic fields $E^{2\omega}$ originate from a nonlinear polarization $P^{2\omega}$ induced by mixing of intense electric fields E^{ω} at frequency ω in the medium, as described by the tensorial equality $P_{\alpha}^{2\omega} = \chi_{\alpha\beta\gamma}^{(2)} E_{\beta}^{\omega} E_{\gamma}^{\omega}$, where $\chi^{(2)}$ is the local nonlinear susceptibility tensor, and subscribes α, β, γ refer to the laboratory coordinates (X, Y, Z). The Einstein's convention for implicit summation of repeated indexes was used. Since the scaffold of a lot of natural soft or hard tissues is composed of fibrils and fibers [20], it is meaningful to assume that the SHG intensity is generated by rod shaped supramolecules of cylindrical C_{∞} symmetry. When Kleinman symmetries [21] are also valid, it can be shown that the nonlinear susceptibility tensor $\chi^{(2)}$ has only two in-

dependent nonvanishing components χ_{zzz} and χ_{zxx}. From these assumptions, the resulting SHG intensity for a given pixel of the image can be written as [10]

$$I(\phi, \psi) = U + V\cos(2\psi - 2\phi) + W\cos(4\psi - 4\phi) \tag{1}$$

when no polarization analysis is performed at detection. The incident laser field propagates along Z axis, and is linearly polarized at angle ψ to X axis (Fig. 2a). The symmetry axis z_χ of $\chi^{(2)}$ is oriented with azimuthal angle ϕ to X axis. The coefficients U, V and W are functions of χ_{zzz}, χ_{zxx}, and are also proportional to the square of both the input intensity I_o and the local concentration $c(r)$ of harmonophores. Explicit expressions for a planar geometry and harmonophores of C_∞ symmetry were given in [10]. Defining $I_\perp \propto [\chi_{zxx} I_o c(r)]^2$ as the intensity measured when the laser polarization is perpendicular to z_χ, we obtained

$$U = \frac{I_\perp}{8}(3\rho^2 + 2\rho + 7) \tag{2}$$

$$V = \frac{I_\perp}{2}(\rho^2 - 1) \tag{3}$$

$$W = \frac{I_\perp}{8}(\rho^2 - 2\rho - 3) \tag{4}$$

where $\rho = \chi_{zzz}/\chi_{zxx}$. This parameter will give us information about the structural organization of the harmonophores (Fig. 2b) within the fibril [15].
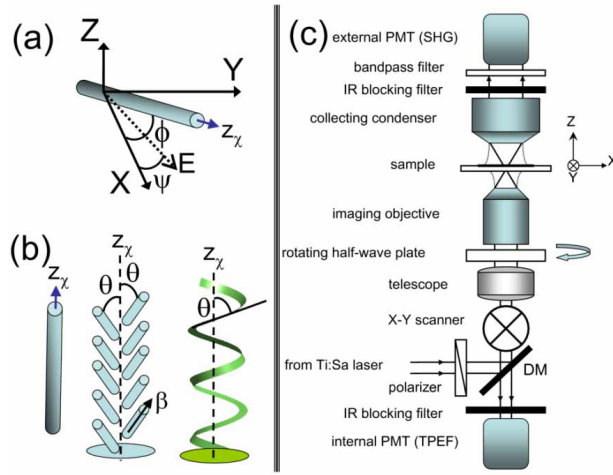

Fig. 2. (color online) : (a) Schematic of a fibril carrying the nonlinear susceptibility $\chi^{(2)}$ in the laboratory frame : laser polarization and C_∞ symmetry axis Z_χ angles with respect to X axis are ψ and ϕ respectively ; (c) Two interpretations of the polar angle θ used to calculate ρ in Eq.(10) for C_∞ harmonophore structures.(c) SHG and TPEF experimental set-up, with laser polarization control. DM= Dichroic mirror, PMT=Photomultiplier Tube.

Equation (1), or equivalent expressions were mainly used to measure the parameter ρ (see for instance [18, 22, 23]), by assuming *a priori* that z_χ is parallel to the apparent fibrils. The value of ρ is derived by fitting with Eq.(1) the mean image intensity as a function of laser polarization. Stoller [10] further used a sophisticated method based on electro-optical modulation of the input laser field to reconstruct the patterns of orientations of z_χ at a micrometric scale

by using a sample scanning experiment. However, the proposed setup cannot be implemented on galvanometer-based scanning microscopes like commercial confocal setups. Moreover the method implicitly assumed that the orientation of z_χ is perfectly correlated to the fibril orientation itself.

In a previous article [17], we simplified the SHG polarization analysis by showing that 2ϕ and ρ can be obtained at each image pixel from the combination of only four images acquired with input linear polarization $\psi_n = n\pi/4$, where n=0,1,2,3. This is the minimum number of images necessary to derive 2ϕ, and the method is analogue to phase cycling in NMR spectroscopy [24]. Letting $I_n(\phi) = I(\phi, \psi_n)$ be the intensity for the nth input polarization state $n\pi/4$, and combining these four intensities, it is easy to obtain from Eq.(1) that

$$
\begin{aligned}
I_{02}(\phi) = [I_0(\phi) - I_2(\phi)]/2 &= V\cos(2\phi) \\
I_{31}(\phi) = [I_3(\phi) - I_1(\phi)]/2 &= V\sin(2\phi)
\end{aligned}
\tag{5}
$$

since the $\cos(4\psi - 4\phi)$ contributions cancel.

The intensity differences $I_{02}(\phi)$ and $I_{31}(\phi)$ fully determine 2ϕ within the interval $[-\pi, \pi]$. Letting $c = \cos(2\phi)$ and $s = \sin(2\phi)$, angle $2\phi = atan2(s,c)$ within $[-\pi, \pi]$ is obtained from the four-quadrant generalized inverse tangent function $atan2$ defined as

$$
\begin{aligned}
atan2(s,c) &= \arctan(s/c) \text{ if } c > 0 \\
atan2(s,c) &= \pi + \arctan(s/c) \text{ if } c < 0 \text{ and } s > 0 \\
atan2(s,c) &= -\pi + \arctan(s/c) \text{ if } c < 0 \text{ and } s < 0
\end{aligned}
\tag{6}
$$

This bijective function $atan2$ within $[-\pi, \pi]$ is a standard ANSI C function, and is implemented in many languages. Since $\phi \in [-\pi/2, \pi/2]$, the orientation is only defined to a multiple of π. This is consistent for cylindrical uniform fibrils. The local orientations are represented in the following figures by symmetrical bars, that are supposed to define the tangent to the fibrils (assuming that the nonlinear susceptibility and the fibril share the same symmetry axis ; this point is further discussed in the subsequent sections).

Therefore, angle 2ϕ is given by I_{02} and I_{31} with the assumption that the sign of V is known. Applying the method to each image pixel leads to an image of the orientation ϕ of the symmetry axis Z_χ of $\chi^{(2)}$. If this symmetry axis coincide with the fibril direction, as will be shown in the next sections, then the image of ϕ directly represents the *orientation field* of the fibril array within the tissue under study. In the following, the method is abbreviated as OF-SHM, for "Orientation Field-Second Harmonic Microscopy".

Since the calculations use differences and ratios of intensities, it avoids problems due to intensity offsets and scaling. It is important to note that ϕ can be determined unambiguously even when the values of U, V, W vary from pixel to pixel, as long as the sign of V remains homogeneous over the image. This property explains the robustness of the estimation of ϕ to slight departures from the hypothesis leading to Eq.(1), such as neglecting birefringence effects. Moreover, ϕ is shifted by $\pi/2$ if the wrong sign is assigned to V. Using Eq.(3) and the results of [10, 22, 23], we observed that in general, $\rho > 1$, that is $V > 0$ for type I collagen, while $\rho < 1$ and $V < 0$ for myosin. Thus, in the following, we use the convention that the orientation angle is given by

$$
\begin{aligned}
\text{if } V > 0, \ 2\phi &= atan2(-I_{31}, -I_{02}) \tag{7} \\
\text{if } V < 0, \ 2\phi &= atan2(I_{31}, I_{02}) \tag{8}
\end{aligned}
$$

for each meaningful pixel, depending on whether the tissue contains collagen or myosin as a major component.

We would like to stress that the apparent sign undetermination of V in our method is equivalent to the choice of the orientation reference in a classical SHG polarization analysis : the orientation of the fibrils is determined from the images to fix a reference angle *before* performing the polarization analysis. The corresponding hypothesis in our method is to fix the sign of V in order to align the orientation field with the apparent orientation of the fibrils deduced from the contrast of the isotropic image. This hypothesis can be applied to determine the sign of V a posteriori if it is not known a priori.

The amplitude of the polarization contrast $|V|$ is estimated by $|V| = \sqrt{I_{02}^2 + I_{31}^2}$, and a polarization-independent image with intensity U can be obtained by averaging pixel by pixel the four previous intensities $U = [I_0(\phi) + I_1(\phi) + I_2(\phi) + I_3(\phi)]/4$. Such an isotropic SHG image was already obtained by Gao et al. [25] by adding three images acquired at input polarizations 0, $\pi/3$ and $2\pi/3$. However, at least four polarizations are needed to recover ϕ. Note that U and $|V|$ depend mainly on the laser power, the local harmonophore concentration and on the $\chi^{(2)}$ tensor components, that is on ρ. Therefore, the ratio $|V|/U$, which is only a function of ρ, leads to estimates of ρ, as will be explained in the last section.

Homemade routines programmed in MATLAB (The MathWorks, Natick, MA) were developed to implement an automated image analysis. Before combining the four images $I_n(\phi)$, three operations were performed : (i) the saturated pixels and pixels of zero values of each of the four polarization images were detected and indexed, which generated four sets of indexes. Therefore, the union with no repetition of these four sets of indexes defines the set of indexes of non relevant pixels, that is where any of the four images is zero or saturated. All these pixels were discarded for the calculation of orientation fields; (ii) the typical salt and pepper noise of SHG images is attenuated with a 3x3 uniform or gaussian filter (note that both filters give the same result) ; (iii) Using the same method as in (i), the pixels where I_{02} or I_{31} are zero or equal to the maximum value are discarded. After calculation of U, V and ϕ, the pixels where the polarization contrast V or mean intensity U are too small with respect to noise can be assigned a special color in the colormap coding of the contrast of the images to highlight doubtful regions of interest.

3. Experimental methods

3.1. *Experimental setup and imaging conditions*

Our imaging setup (Fig. 2c) was based on a modified confocal microscope composed of an Olympus IX71 inverted stand and a FluoView 300 scanning head (Olympus, Hamburg, Germany). A femtosecond Ti:sapphire laser (Mira900-Verdi5 combination, Coherent, Saclay, France) was coupled to the microscope and was tuned at a wavelength of 810 nm for all experiments. Linearly polarized 200-fs pulses at a repetition rate of 76 MHz with average powers <50 mW were sent to two different microscope objectives :(i) a low numerical aperture (NA) model (10x-NA0.25, Leitz Wetzlar) ; (ii) a high-NA water-immersion model (UplanApo/IR 60xW NA1.2, Olympus). The 60x objective was slightly underfilled by the input laser beam so as to adapt the divergence of the second harmonic emission to the aperture of the collection optics. The SHG light was collected in the forward direction by either a 0.3 NA condenser (IX-ULWCD, Olympus) or a 0.9 NA water-immersion condenser (IX2-TLW, Olympus) to fit with the 10x or 60x objectives respectively. The illumination wavelength was blocked by a 2-mm thick BG39 filter (Lambda Research Optics, CA). The SHG was detected through a 405-nm (10-nm full width half-maximum) bandpass filter (Edmund Optics, York, UK) by a compact external photomultiplier tube (PMT) assembly (H5783-01, Hamamatsu Photonics, Massy, France). The PMT assembly was connected to a transimpedance amplifier (C7319, Hamamatsu) so as to match the SHG detection to the internal PMTs of the microscope and

to use the full range of FluoView hardware and software. The laser polarization was rotated to the four needed orientations by a zero-order half-wave plate (Edmund Optics, UK), mounted in a motorized rotation stage (PR50CC, Newport). The stage was inserted in the place of the fluorescent cube turret of the microscope, next to the objective entrance pupil. The TPEF light was epicollected by the microscope objective, passed the scan mirrors and was detected by one of the two descanned channels of the confocal microscope. The confocal pinhole was removed from the detection path since two-photon excited fluorescence is inherently localized at the objective focal volume. The excitation wavelength was blocked by a dichroic mirror in the scanning head (675dcxru, Chroma Technology, Rockingham, VT, USA) and a 2-mm thick BG39 filter in front of the internal PMT. Full-field TPEF and SHG images with 12-bit intensity resolution were acquired from FluoView microscope software, then recorded as TIFF files. The scan speed was fixed at its lowest value corresponding to 2.68 s per frame ($10.2\mu s$ per pixel for 512x512 images).

Sample preparation

Fresh sheep tendons, and veal cutlets were directly obtained from the butcher the morning of the experiment days. Then, 100 or 200-μm thick sections were cut from the middle of the tendon, or from the veat muscle, and placed between a microscope slide and a 170-μm-thick cover-glass. To avoid dehydration, the edges of the cover-glass were sealed with nail polish.

Fertilized chick eggs (gallus gallus) were incubated in humidified atmosphere at $37\,^\circ$C until the needed age. The albumen was drained out from a hole in the blunt-end of the egg's shell before opening a square window in the shell. The embryo was then rescued and washed in a phosphate buffer solution (PBS), and staged according to Hamburger and Hamilton (HH) [26]. A part of the embryo's muscles or head were extracted and spread over a cover-glass before performing TPEF/SHG experiments.

4. Collagen and myosin fibril orientations

4.1. Sheep tendon collagen

As a first example of application of our OF-SHM method to a dense tissue, we choose tendon (here sheep tendon) sections for the following reasons. First, type-I collagen accounts for 65-80% of the dry mass of tendons, and gives a strong SHG signal. Second, the subfascicular units consist of fibres, fibrils and microfibrils of collagen, that can be easily identified at different hierarchical levels. Depending on the region of interest and imaging scale, a wavy organization of the fibrils or microfibrils can be detected, but the microfibrils are mostly arranged into parallel bundles. Thus the structural organization of tendon insures a high microfibril concentration, with only small spatial defects that preserve a high optical coherence between the generated SHG signals, resulting in a very high overall SHG signal.

Figure 3 presents high magnification (60x objective) SHG images of a non uniform region, that exhibits well separated fibrils with various orientations. The estimated lateral w_{xy} and axial w_z extents of the two-photon Point Spread Function (PSF) [4] are 0.4μm and 2μm respectively. The value of w_{xy} matches approximately the pixel size. The four images in Fig. 3(a1-a4) show how the SHG contrast varies with laser polarizations. The polarization contrast is rather high, as expected for a sample with a high degree of order. The isotropic image U obtained by averaging the four images is presented in Fig. 3(b). From the value of w_z of our high-NA objective, it can be deduced that the observed fibrils are mainly in the image plane : the typical length of the fibrils being larger than 40μm, the maximum out-of-plane angle is $\approx 1/20$ rad $< 3\,^\circ$. Thus, we mainly studied the orientation of the symmetry axis of the nonlinear susceptibility of fibrils lying in the focal plane. The corresponding orientation field derived from Eqs.(5,6,7) is shown in Fig. 3(c), where a small bar centered on the Region of Interest (ROI) represents the local

orientation ϕ. This orientation has to be compared with the apparent orientation of the fibrils as they appear in Fig. 3(b).
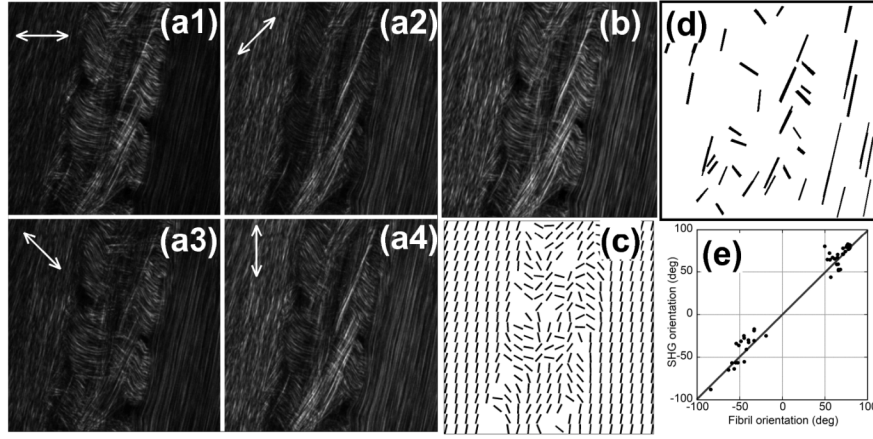

Fig. 3. SHG of sheep tendon collagen (60xW-NA1.2 objective, 512x512 images, full scale 235μm). (a1-a4) Acquisition with four polarizations indicated by the double white arrows; (b) isotropic image; (c) Orientation field represented by bars directed along the symmetry axis of the nonlinear susceptibility (one bar for each bloc of 16x16 pixels); (d) Masks selecting different fibrils; (e) Correlation between the apparent orientation of the fibrils (abscissa) and the orientation of the principal axis of the SHG nonlinear susceptibility (ordinate).

A quantification of the correlation between the two orientations is performed as follows. We assumed that possible Moire effects due to the fibrillar nature of the sample, and subtle SHG coherent effects, do not cause significant errors in the apparent fibril orientation as seen from the isotropic image U. Under this assumption, apparent fibrils are manually selected by rectangular ROIs to create elongated masks M, that are presented in Fig. 3(d). Then, for each mask, we calculated : (i) the mean direction of the rectangular mask; (ii) the mean orientation angle ϕ_M of the SHG nonlinear susceptibility axis within the mask. Circular Statistics [27] gives the following formula

$$\phi_M = \frac{1}{2} atan2 \left(\frac{\sum_{\alpha,\beta \in M} \sin(\phi_{\alpha\beta})}{\sum_{\alpha,\beta \in M} \cos(\phi_{\alpha\beta})} \right) \tag{9}$$

where the summations are performed over all the pixels within the mask. The results are presented in a correlation plot between the supposed fibril orientations and the mean directions of the SHG symmetry axis on Fig. 3(e). The data are well aligned on the bissectrix, with the square of the correlation coefficient $R^2 \approx 0.97$. This high R^2 value demonstrates that the OF-SHM method provides fibril orientation with a good reliability. These results are fully consistent with our previous study, performed at the same scale, on isolated collagen fibrils in rat liver [17], and extend its applicability to dense systems.

An important question is whether at lower magnification and resolution, OF-SHM polarization allows the reconstruction of orientation fields of the fibrillar structure even if individual fibers cannot be resolved. The interest of our method for the study of dense systems is illustrated in Fig. 4, where large scale images of sheep tendon were obtained using the 10X objective ($w_{xy} \approx 1\mu$m and $w_z \approx 10\mu$m).

The method was tested by using two orientations of the sample, which was physically rotated in the image plane by 20$°$ with respect to the initial direction. The ROI shown in Fig. 4 give rather uniform images, where no fibrils can be resolved. Although the contrast is sufficient to

recognize by eye the main fibril orientation, it is rather low. Thus performing image analysis to obtain a local orientation distribution may be difficult, as shown for instance by the high degree of complexity of the reconstruction algorithms used to analyze collagen fiber orientation from linear microscopy images [28]. Moreover, such algorithms only give an indirect measurement of the fiber orientation based on an intensity contrast that is not related to the intrinsic optical anisotropy of the system. On the contrary, the OF-SHM analysis directly gives the orientation of the fibers.
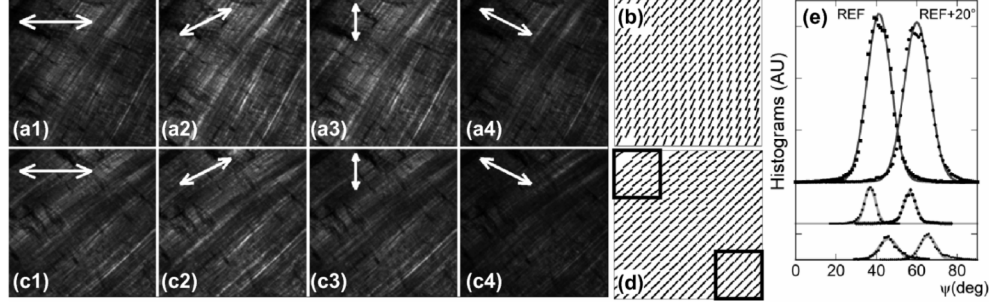

Fig. 4. SHG of sheep tendon collagen (10x-NA0.25 objective, 256x256 images, full scale 625μm). (a1-a4) 4 polarization images for the reference orientation. (b) Orientation field of the a-image by blocks of 16x16 pixels. (c1-c4) 4 polarization images of the sample that was physically rotated by $20°$; (d) Orientation Field of the c-image; (e) Histograms of the orientations. For clarity, the different histograms were vertically shifted : (Top) histograms for all the pixels of the image; (Middle and Bottom) Histograms of the 80x80 ROI at the top left and bottom right corners of the image respectively; The histograms were normalized with a weight corresponding to the size of the ROI. Continuous lines are gaussian fits.

The normalized histograms of the orientation for all 256x256 pixels of the two images corresponding to the two sample orientations are presented in Fig. 4(e). For circular distributions, the analogue of the gaussian distribution is the von Mises [27] distribution $w(\psi) \sim \exp(\kappa \cos(\psi - \psi_m))$, where large concentration parameter κ indicate small orientation disorder around the mean direction ψ_m. When $\kappa \gg 1$, it is is well approximated by a gaussian $\sim \exp[(\psi - \psi_m)^2/2\sigma_\psi^2]$ with $\kappa = 1/\sigma_\psi^2$. Both distributions were used to fit the data by a least-square method, and give almost indistinguishable results with a square of the correlation coefficient $R^2 \approx 0.992$ for the two orientations. The best fitting parameters were found to be $\psi_m = 41.3° \pm 0.1$, $\sigma_\psi = 6°$ and $\psi_m = 60.1° \pm 0.1$, $\sigma_\psi = 6.3°$ for respectively the reference orientation and the one rotated by $20°$. For both orientations, the angular dispersions are identical, while the mean angle is modified by the rotation angle, as expected.

The observed angular dispersion $\sigma_\psi \approx 6°$ is due to at least two contributions : (i) disorientation of the fibrils due to the natural crimp of collagen fibrils ; (ii) angular noise coming from the method. As indicated by Fig. 4(b) and (d), regions of different orientations can be distinguished in the whole image. To try to unravel the different contributions, we also select ROIs of 80x80 pixels. We expect the first contribution to decrease as the distribution of the orientation of the fibrils becomes more peaked while the second one should not vary. The corresponding histograms are presented in Fig. 4(e). Again, the mean angles of both ROIs are shifted by $20°$. Since the lowest dispersion value was $\psi_m \approx 3°$, we can infer that the contribution of the OF-SHM method to the angular dispersion is around $3°$. These results confirm the potentiality of OF-SHM to measure orientation fields when the fibrils cannot be resolved.

4.2. Myosin in veal muscle and chicken embryo

Muscles are organized in fiber bundles, the fiber itself being organized hierarchically. It contains hundreds of parallely aligned myofibrils, laterally interconnected by intermediate filaments. Each myofibril consists of serially connected sarcomeres, the structural and functional unit in a muscle fiber, and its length is an important feature for contraction analyzes. The structural organization of the 3D myofibril array, with series and parallel connections, is an important parameter to understand muscle properties. The fibrous protein myosin is a good nonlinear optical source, that gives the opportunity to study muscles by SHG microscopy. In this part, we will focus only on the validation of OF-SHM microscopy to myosin containing samples, with the study of a chicken embryo muscle, and by reconsidering the case of veal meat with regards to the problem pointed out in the introduction.

For the chicken embryo, myofibrils start to be formed from the 6th day of incubation. After the 8th day of incubation, these myofibrils start to coalesce between them to form muscular cells [29]. Figure 5 presents a longitudinal section of a striated muscular tissue dissected from the back of a 6-7th days of incubation chicken embryo, and imaged with a 10x-NA0.25 objective. Three bundles of myosin filaments are presented, and the SHG contrast comes from myosin. This point can be confirmed by remarking that only $V < 0$ gives an orientation field (Fig. 5(c)) that fits the orientation of the apparent fibrils as seen on the isotropic image of Fig. 5(b). The important point shown by Fig. 5(b) is that each bundle contains a series of myofibrils arranged in an almost parallel fashion. The myofibrils can be well resolved, and the mean interfibril distance was estimated to be $\sim 15\mu$m. This is consistent with the fact that at this stage of the development, myofibrils are not fused yet between them in order to form muscular cells.
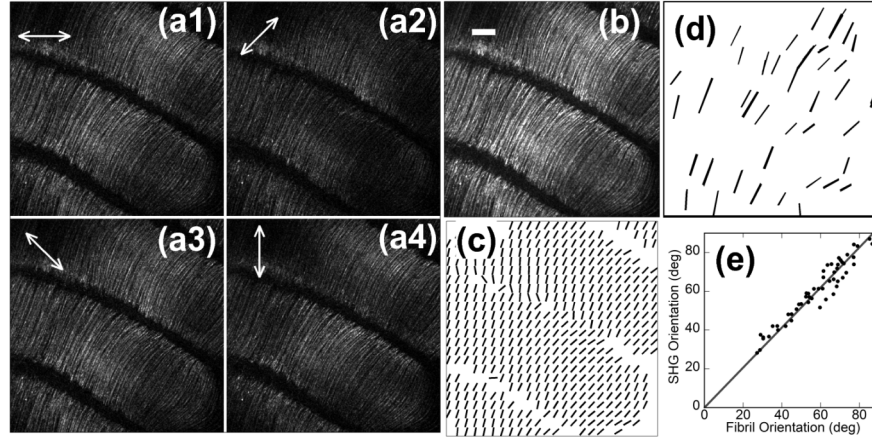

Fig. 5. SHG images from myosin of the muscle of the back of a 7 days chicken embryo (10x-NA0.25 objective, 768x768 images, full scale 938μm). Scale bar : 100μm. The legends are similar to Fig. 3.

Since the myofibrils can be easily distinguished in the chicken embryo, we performed the same analysis as the one done for collagen in the previous section. The orientation field shown in Fig. 5(c) well reproduces the myofibrillar patterns of Fig. 5(b). A linear correlation between myofibril orientations, as exemplified by the masks presented in Fig. 5(d), and the SHG axis is given in Fig. 5(e). The data overlap well the bissectrix. A linear regression where the line fit is forced to zero gives a slope of 1.03 very close to unity, with $R^2 \approx 0.93$. This example demonstrates that OF-SHM also provides reliable orientation fields for myosin.

In the adult case, myofibrils fuse to form a muscular cell. Figure 6 shows a striated muscular

tissue from a veal escalope at high magnification (60x), that appears smoother than the muscle in the embryonic case. We then reconsidered the orientation field of veal muscle obtained by using 10x and 60x magnifications. The orientation field of Fig. 6(c) at 10x magnification follows the apparent flow of myofibrils as seen on TPEF and SHG images of Fig. 6(a) and (b) respectively. A good agreement is still observed at the higher 60x magnification, as shown in Fig. 6(d,e,f).
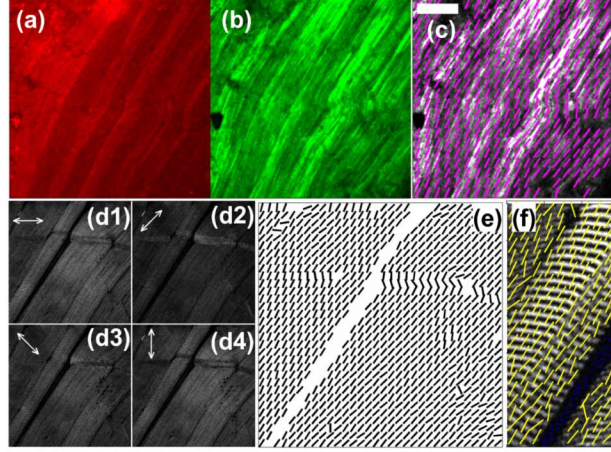

Fig. 6. (Color online) TPEF, myosin SHG and orientation field of veal muscle at two scales. First raw: 10x-NA0.25 objective, 400x400 images, scale bar 100μm. (a) TPEF; (b) SHG; (c) Orientation field superimposed on the isotropic SHG image. Second raw : 60xW-NA1.2 objective, 1024x1024 images, full scale 235μm; (d1-4) 4 polarization images; (e) Orientation Field; (f) Detail of the orientation field with superimposed isotropic SHG image.

As explained in the introduction, the direction of the myofibrils may not be perpendicular to the striated structure due to the sarcomeres. This point is clearly illustrated in Fig. 6(f), that shows a striated structure that is not perpendicular (116°) to the principal direction of the myofibril bundle, as indicated either by the bundle border or by the average direction of z_χ obtained by OF-SHM. This observation raises the question of the extrinsic or intrinsic origin of this $\sim 30^\circ$ misorientation. Extrinsic origins may come from the physical and optical sectioning of the myofibril bundles. For the intrinsic origin, we propose the following interpretation. If the myofibrils are all packed parallel to a given direction with the same starting point, then the sarcomeres will be in phase with each other, and the dark bands will appear perpendicular to the packing direction. However, if the fibrils are shifted by the same increment from each other, the fibrils staying still parallel, the dark bands will be no longer perpendicular to the myofibril orientations. This example points out the interest in measuring the orientation field to interpret images provided by second harmonic microscopy.

5. Ratios ρ of the nonlinear susceptibility components for collagen and myosin

Besides the orientation of the symmetry axis of $\chi^{(2)}$ that is collinear to the fibril axis, we would like to show in this section that our OF-SHM method can provide an estimation of $\rho = \chi_{zzz}/\chi_{zxx}$. This is an important quantity that contains some structural informations about the local organization of harmonophores in the supramolecule that gives rise to SHG. For our case of interest, and under the assumption that the nonlinear susceptibility is built from the arrangement of harmonophores with axial symmetry (Fig. 2b), and that the microscopic hyperpolarizability tensor of each harmonophore can be well approximated by a single dominant component β, then ρ

is related to the polar angle θ of the principal axis related to β with respect to the mesoscopic axial symmetry axis z_χ, by [23]

$$\rho = 2/tan^2\theta \qquad (10)$$

The influence of polar disorder was also considered in [22, 30]. From Eq.(4), the ratio V/U is independent of the laser intensity, harmonophore concentration, and reads

$$\frac{V}{U} = \frac{4\left[\rho^2 - 1\right]}{\left[3\rho^2 + 2\rho + 7\right]} \qquad (11)$$

As ρ varies from 0 to $+\infty$, $V/U(\rho)$ is a increasing function varying between -4/7 and 4/3. Eq.(11) can be inverted to give $\rho > 0$ as

$$\rho = \frac{r + 2\sqrt{4(1+r) - 5r^2}}{4 - 3r} \qquad (12)$$

where $r = |V|/U$ under the hypothesis that $\rho > 1$ and $r = -|V|/U$ if $0 < \rho < 1$, since only the absolute value $|V|/U$ can be measured from our 4-polarizations analysis.
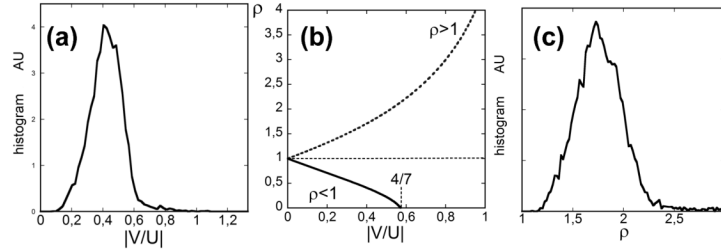

Fig. 7. Relationship between $|V|/U$ and ρ from Eq.(12).(a) Histogram of $|V|/U$ for sheep tendon collagen obtained from a 512x512 image acquired with an 60xW-NA1.2 objective; (b) Theoretical relationship Eq.(12) between ρ and $|V|/U$ when $0 < \rho < 1$ or $\rho > 1$; (c) Histogram of ρ values corresponding to the $|V|/U$ values of Fig. 7(a).

The evolution of ρ as a function of $|V|/U$ is presented in Fig. 7(b). When $\rho > 1$ (or $|V|/U$ becoming closer to 4/3), ρ is a very strongly increasing function of $|V|/U$. The relationship is almost linear for small values of $|V|/U$. In calculating ρ from Eq.(12), the values of $|r|$ that are not in the range $0 < |r| < 4/7$ when $\rho < 1$ and $0 < |r| < 4/3$ when $\rho > 1$ should be discarded. The discrepancy between the measured $|V|/U$ values and these limits are generally due to noise, simplifying assumptions (for instance the hypothesis $\chi_{31}/\chi_{15} = 1$ may not be exactly verified) and also limitations of the model that does not take into account of sample birefringence and axial field components in the vicinity of the geometrical focal point. Note that these assumptions are more compelling for the estimate of ρ than for the estimation of ϕ that does not depend on the value of the coefficients U, V, and W, but only on the sign of V. The transformation of the histogram of $|V|/U$ in Fig. 7(a) into the histogram of ρ in Fig. 7(c) using Eq.(12) is also illustrated using the data of a SHG image of collagen from sheep tendon.

In the following, we analyze the distribution of ρ over several samples of collagen and myosin. We made the hypothesis that $\rho > 1$ and $\rho < 1$ for collagen and myosin respectively.

The mean ρ value, denoted as $< \rho >$, and standard deviation σ_ρ can be calculated from raw data, and the results are summarized in Table 1. We used Eq.(10) to calculate the polar angles corresponding to the values of ρ. However, in order to obtain symmetric confidence

Figure	Obj	$<\rho>\pm\sigma_\rho$	$\bar{\theta}\pm\Delta\theta$ (deg)
Collagen sheep tendon	60xW-1.2	1.8 ± 0.3	46.7 ± 2.4
Collagen sheep tendon	10x-0.25	1.6 ± 0.2	48.3 ± 1.8
Collagen chicken head (HH 8)	10x-0.25	1.7 ± 0.36	47.7 ± 3
Collagen chicken skin (HH35)	10x-0.25	1.4 ± 0.3	50 ± 3
Myosin veal muscle	60xW-1.2	0.6 ± 0.2	61.8 ± 4.1
Myosin veal muscle	10x-0.25	0.6 ± 0.15	61.6 ± 3
Myosin chicken back	10x-0.25	0.5 ± 0.1	63.6 ± 2.3

Table 1. Mean values of ρ for collagen and myosin. $<\rho>$ and σ_ρ are respectively the mean and standard deviation of ρ calculated directly from the raw data with usual formula. The polar angle $\bar{\theta}$ and its incertitude $\Delta\theta$ were calculated as explained in the text.

interval for angle θ, we defined $\theta_\pm = \text{atan}(\sqrt{2/(<\rho>\pm\sigma_\rho)})$, and used $\bar{\theta} = (\theta_+ + \theta_-)/2$ and $\Delta\theta = |\theta_+ - \theta_-|/2$. These results are also reported in Table 1 as $\bar{\theta}\pm\Delta\theta$.

Though the measured values of ρ , as well as the corresponding polar angles θ, are in good agreement with the values reported in literature [10, 11, 15, 18, 22, 23], the error bars are larger than in conventional procedures using more than four polarization states and an intensity averaging over many pixels. It is due to the non redundancy of our 4-polarization method. We also verified that the results are almost independent of the NA value of the objective used for collagen in sheep tendon, since the confidence interval of both values superimpose.

6. Conclusion and perspectives

In the present study, we have shown that only four SHG images are necessary and sufficient to estimate the local orientation of the principal axis of the nonlinear susceptibility tensor $\chi^{(2)}$ of collagen and myosin, that was proved to be strongly correlated to the fibril orientation. Moreover, the data also lead to an estimation of the ratio ρ of the two non-vanishing components of $\chi^{(2)}$. Our study shows that the method works well for non-dense and dense arrays of collagen or myosin fibrils. Thus OF-SHM gives the opportunity to reconstruct the orientation fields of collagen and myosin fibrils within tissues, with minimum measurement time and photodamage.

The method still have some room for improvements, both to reduce experimental errors as well as improving the interpretation of orientational fields, and automation. Current work are under progress to further increase the amount of information that can be derived from OF-SHM.

By way of perspectives, we present two preliminary applications of orientation field measurements to chicken embryology. The first example, presented in Fig. 8, concerns the formation of feather buds [31]. As shown in Fig. 8(c), the orientation field in the inter-bud region is homogeneous, and along the main orientation of the fibroblasts that are delineated by collagen fibers as seen in Fig. 8(b). Within the buds, a singularity appears and the orientation field appears radial.

The second example, reported in Fig. 9, reveals the orientation field within the head of a HH8 chicken embryo. The superposition on Fig. 9(c) of isotropic TPEF and SHG images of Figs.9(a) and (b) respectively, shows that the fluorescent contribution (TPEF) embodies the collagen component (SHG). The SHG intensity is stronger along the border of the embryo, indicating a higher collagen concentration that probably corresponds to an outgrowth or a folding of the mesoderm at the boundary. The collagen fibrils also appear to organize perpendicular to the embryo border, as shown by the reconstructed orientation field of Fig. 9(d). This is consistent with the fact that the part of the embryonic ectoderm intended to form the brain and the spinal-cord (neural plate) is rolled up and inserted under the skin to form the mesoderm. At the end of this stage, new cells of the mesoderm intercalate between the first invaginated cells and will be aligned together in the same direction of migration perpendicularly to the neural crest [32].
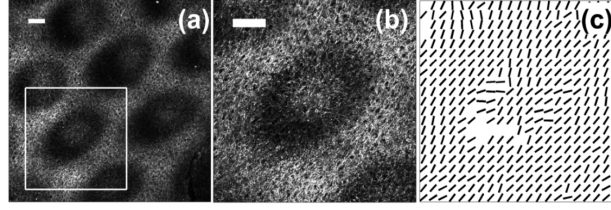
Fig. 8. SHG images of the skin of a 9 days (HH35) chicken embryo (10x-NA0.25 objective).(a) Full scale SHG image (1024x1024) ;(b) Zoom of the ROI delineated by the white rectangle (512x512 image) ;(c) Orientation field. Scale bars : 100μm.
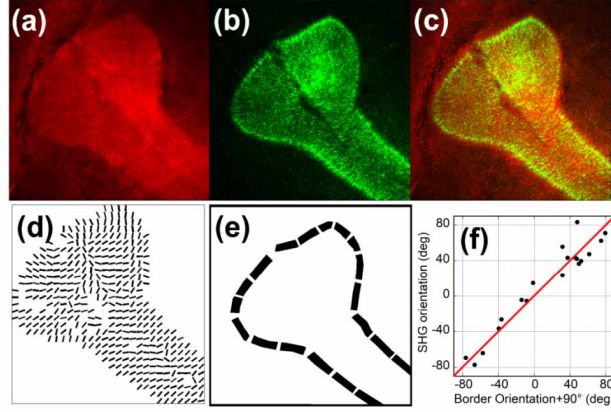

Fig. 9. (color online) Head of a HH8 Chicken Embryo imaged with a 10x-NA0.25 objective (700x700 image, 940x940μm^2). (a) TPEF (Red) ;(b) Collagen SHG (green) ;(c) TPEF+SHG ;(d) Orientation field ;(e) Masks delineating the border of the embryo ;(f) Correlation between the SHG and masks orientations, corrected by 90°.

That collagen fibrils are perpendicular to the embryo border can be proved from the analysis of the orientation field of collagen fibrils along the border of the embryo, as shown by Fig. 9(d-f). The orientation orthogonal to rectangles delineating the embryo border and the corresponding orientation of z_χ are well correlated ($R^2 \approx 0.925$) (Fig. 9(f)). In other words, the collagen fibrils are in the same direction as the fibroblasts of the mesoderm, that produce the collagen in the extracellular matrix. Further work is under progress to study the evolution of orientation fields in the chicken embryo as a function of development, at various spatial scales.

In summary, our method named Orientation Field-Second Harmonic Microscopy or OF-SHM, thus provides a nondestructive and potentially noninvasive technique to perform in-depth imaging of nonlinear fibrillar structures (collagen, myosin,...), and to evaluate the structural organization typical of healthy or diseased tissues. OF-SHM applies up to a few hundreds micrometers in depth, and does not necessitates staining since it uses endogenous signals. Other applications of OF-SHM may cover analysis of liver or lung fibrosis, skin pathologies, soft tissue or muscle scarring, neuromuscular diseases, electrophysiology...

Acknowledgments